Shi *et al. Journal of Translational Medicine* (2026) 24:308
https://doi.org/10.1186/s12967-026-07780-4

Journal of Translational Medicine

RESEARCH Open Access

Logic-gated fluorescent biosensor integrating aptamer recognition and oxidative cleavage-responsive DNA circuit for myeloperoxidase detection

Bo-Yu Shi[1†], Jia-Mei Zhang[1†], Si-Han Qin[1], Han-Ye Yuan[1] and Jing Wang[1*]

Abstract

Background Precise discrimination between protein abundance and catalytic activity of proteases remains a critical yet challenging objective in biomedical diagnostics due to overlapping biological functions, intricate regulatory mechanisms, and extensive interference from endogenous biomolecules.

Methods Herein, we report a novel dual-lock DNA biosensing platform, exemplified through myeloperoxidase (MPO), which concurrently integrates aptamer-mediated molecular recognition and hypochlorous acid (HOCl)-triggered oxidative cleavage to rigorously assess both MPO protein expression and enzymatic functionality. Specifically, MPO interaction with a conformationally structured DNA aptamer facilitates selective release of a trigger strand, while HOCl, produced enzymatically by active MPO, cleaves a strategically phosphorothioate-modified hairpin structure. Only upon simultaneous fulfillment of these two molecular conditions does the sensing mechanism activate a downstream catalytic hairpin assembly (CHA), achieving significant signal amplification.

Results This stringent AND logic gate configuration markedly suppresses false positives and nonspecific background signals, demonstrating exceptional reliability across diverse and complex biological samples including serum, saliva, and cellular lysates.

Conclusions The proposed biosensing strategy thus provides a versatile, accurate, and broadly applicable analytical tool for simultaneous quantification of protease content and functional activity, holding considerable promise for advancing clinical diagnostics and pathological investigations.

†Bo-Yu Shi and Jia-Mei Zhang contributed equally to this work.

*Correspondence:
Jing Wang
wangjing822@tmu.edu.cn
[1]Department of Clinical Biochemistry and Molecular Diagnostics, College of Medical Technology, Tianjin Medical University, Tianjin 300203, P. R. China

Introduction

Accurate determination of both protease abundance and catalytic activity is essential in biomedical diagnostics but remains technically challenging [1–3]. Proteases regulate key biological processes, including inflammation, immune responses, and disease progression [4]. However, their analysis in complex biological matrices is hindered by overlapping substrate specificities, complex activation pathways, and interference from endogenous biomolecules. Consequently, conventional assays often provide incomplete or misleading information [5]. Most existing protease assays measure only a single analytical dimension. Immunoassays quantify total protein levels but do not reflect enzymatic activity, whereas activity-based assays report catalytic function without distinguishing between active and inactive enzyme forms. This disconnect complicates data interpretation, particularly in pathological conditions where protein expression and enzymatic activity are poorly correlated.

Myeloperoxidase (MPO), a lysosomal heme-containing peroxidase predominantly expressed in neutrophils and monocytes, exemplifies this analytical challenge. MPO is implicated in oxidative stress–related diseases, including atherosclerosis, neurodegenerative disorders, and chronic inflammatory conditions [6–9]. It catalyzes the oxidation of chloride ions (Cl^-) by hydrogen peroxide (H_2O_2) to generate hypochlorous acid (HOCl), a potent oxidant essential for antimicrobial defense and inflammatory regulation [10, 11]. Dysregulated MPO activity can lead to tissue damage, highlighting the need to differentiate between MPO protein levels and catalytic activity [12–18]. Current MPO detection methods, including immunoassays and enzymatic activity assays, typically provide single-dimensional information [19–22]. These approaches suffer from nonspecific interference, limited sensitivity in complex samples, and poor discrimination between active and inactive MPO. Moreover, activity-based assays often exhibit cross-reactivity with other peroxidases, such as horseradish peroxidase (HRP) and lactoperoxidase (LPO), which reduces analytical specificity [23–25].

Herein, we report a dual-lock DNA logic-gated biosensor for the simultaneous evaluation of MPO abundance and catalytic activity. The sensing strategy integrates aptamer-mediated MPO recognition with HOCl-responsive oxidative cleavage of a phosphorothioate-modified DNA hairpin [26–30]. Signal amplification is triggered only when both events occur, forming a strict AND logic gate. Catalytic hairpin assembly (CHA) is used as a representative amplification strategy to demonstrate feasibility [31–33]. This dual-lock design improves specificity, suppresses false-positive signals, and enhances analytical reliability in complex biological environments.

Results and discussion

Design of the dual-lock DNA logic-gated circuit

We designed a dual-lock DNA logic-gated sensing circuit in which a catalytically controlled catalytic hairpin assembly (CHA) reaction is activated only when two independent molecular conditions are satisfied (Scheme 1). This design employs two orthogonal control modules to achieve high specificity and signal fidelity. The first lock is based on an aptamer–trigger strand duplex. In the absence of target protein, the trigger strand (T) is partially hybridized with the aptamer (Apt), forming a stable complex that sequesters T and prevents downstream activation (Scheme 1a). When MPO is present, it binds to the aptamer with higher affinity than the T strand, leading to competitive displacement and release of T. This process unlocks the first gate and exposes the toehold domain of the trigger strand, allowing it to initiate subsequent strand displacement reactions. The second lock is encoded in a phosphorothioate (PS)-modified hairpin precursor (pH2), which represents an inactive form of hairpin H2. A PS modification is introduced at a defined position within the stem region of pH2, serving as a chemically responsive blocking site. This modification is selectively cleaved by hypochlorous acid (HOCl), which is generated by MPO in the presence of H_2O_2 and Cl^-. Upon HOCl exposure, oxidative cleavage at the PS site disrupts the blocking structure and converts pH2 into the active H2 form, thereby exposing its toehold domain (Scheme 1b, Figure S1). Only when both locks are released does the CHA reaction proceed. The liberated T strand first interacts with hairpin H1 through toehold-mediated strand displacement, forming an intermediate complex. The activated H2 then displaces the trigger strand from the H1–T duplex, producing a stable H1–H2 complex and regenerating free T for further catalytic cycles (Scheme 1c). This cyclic process results in efficient signal amplification. The formation of the H1–H2 duplex ultimately induces structural changes in a fluorogenic probe, generating a measurable fluorescence signal. In this system, MPO binding serves as the first molecular key, while HOCl production functions as the second. Only their simultaneous presence activates the full CHA cascade, yielding a strict AND-gated signal output with high specificity and resistance to background interference.

Functional validation of the dual-lock logic-gated DNA circuit modules

To validate the functionality of each module within the proposed dual-lock logic-gated sensing system, we systematically examined three critical components: trigger strand (T) release, HOCl-mediated activation of the protected hairpin pH2, and signal amplification via CHA (Fig. 1). In Fig. 1a and b, we first verified the mechanism

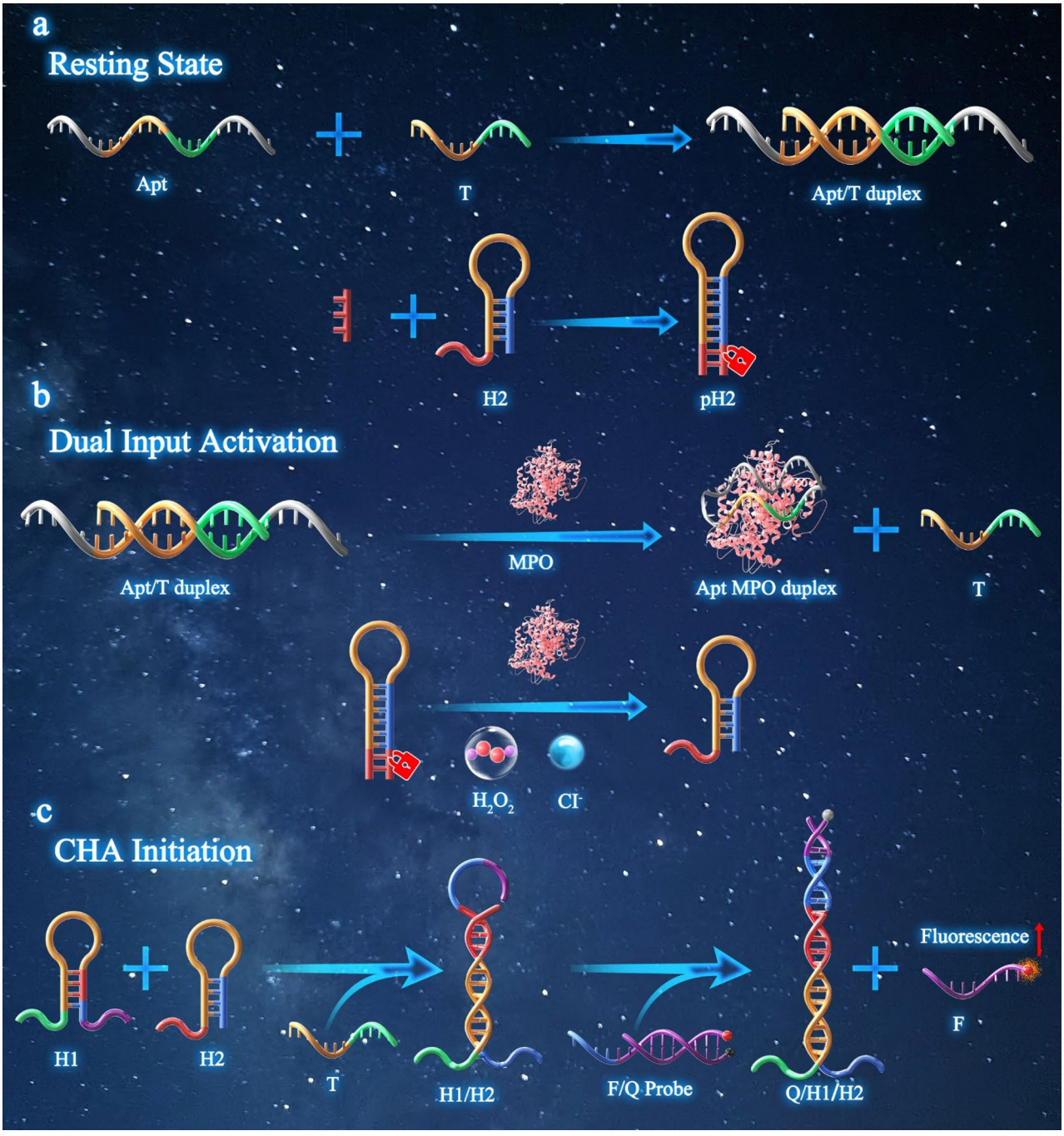

Scheme 1 Schematic of the logic-gated DNA circuit for MPO detection. The system integrates aptamer recognition and HOCl-responsive activation to enable concurrent evaluation of MPO content and enzymatic activity. (**a**) In the resting state, the trigger strand (T) is hybridized with the MPO-specific aptamer, while H2 remains in an inactive precursor form (pH2) containing an internal PS site. (**b**) MPO binding displaces T from the aptamer, and MPO-generated HOCl cleaves the PS site in pH2, converting it into active H2 with an exposed toehold. (**c**) Only when both T and active H2 are present is the CHA circuit initiated, leading to fluorescence output

of the first lock, which is based on the displacement of the T strand from its duplex with the aptamer (Apt). The Apt and T strands were hybridized in a 1:1 molar ratio, with the Apt labeled at the 5′ end with a Cy3 fluorophore and the T strand labeled with a BHQ2 quencher. In the initial Apt/T duplex, fluorescence was effectively quenched. Upon addition of varying concentrations of MPO, fluorescence intensity increased proportionally, whereas the signal remained low in the absence of MPO. These results confirm that MPO can specifically bind the aptamer and displace the T strand, thereby unlocking the first gate and initiating signal transduction

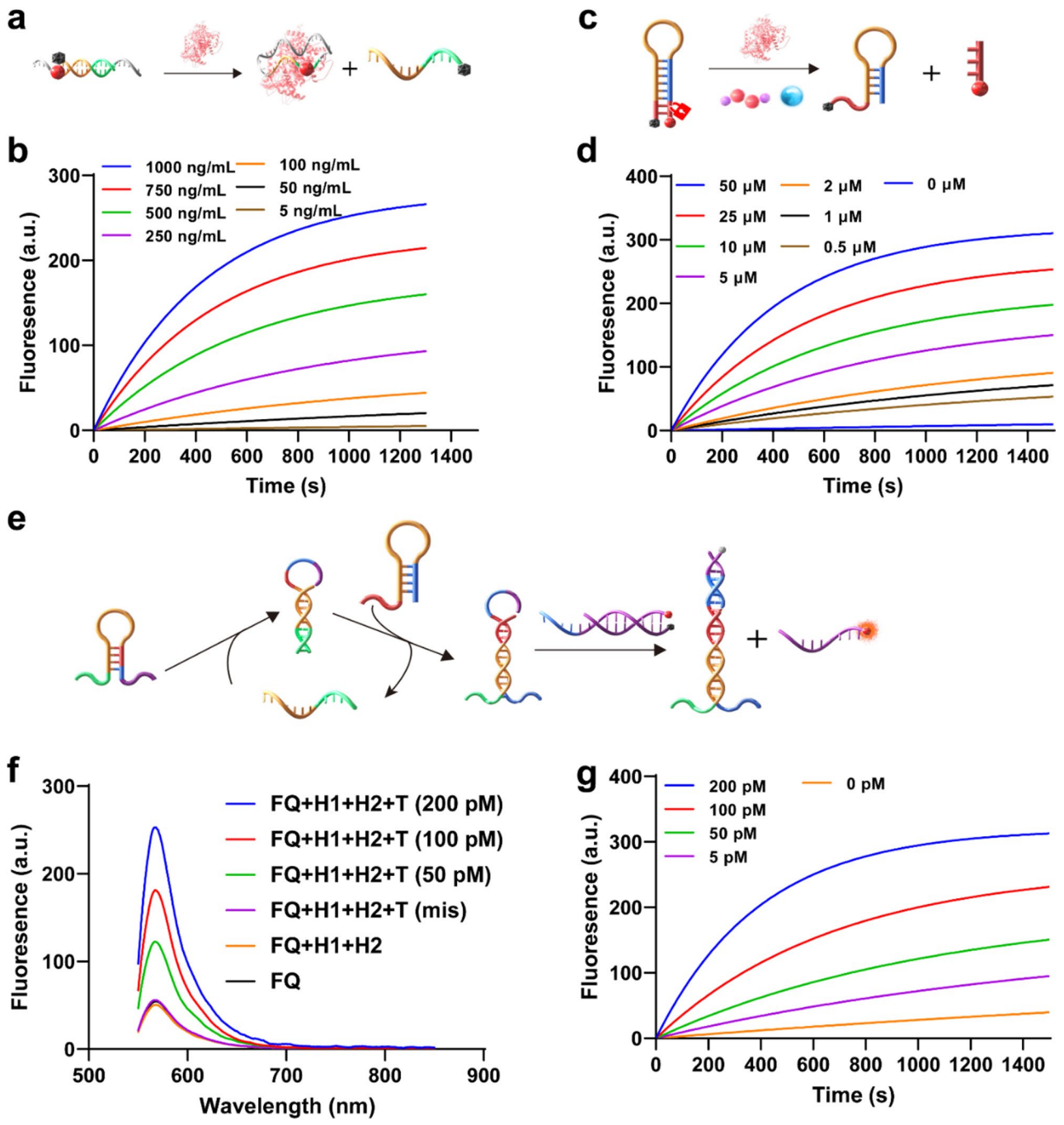

Fig. 1 Functional validation of the dual-lock logic-gated sensing system. (**a**) Schematic illustration of the first gate: MPO binding induces aptamer conformational change, releasing the quenched trigger strand (T). (**b**) Fluorescence recovery of Cy3-labeled Apt/T duplex with increasing MPO concentrations (5–1000 ng/mL). (**c**) Schematic of the second gate: HOCl cleaves the PS site in pH2, converting it to active H2. (**d**) Fluorescence kinetics of pH2 activation under various HOCl concentrations (0–50 μM). (**e**) Schematic of CHA initiated by released T and H2, leading to FQ probe activation. (**f**) Fluorescence spectra of CHA triggered by different T concentrations (200–50 pM), mismatched T, and control. (**g**) Time-dependent fluorescence curves of CHA with increasing T input

through toehold exposure. In Fig. 1c and d, we evaluated the second lock—the HOCl-responsive activation of the protected hairpin pH2. This structure contains an internal PS cleavage site, allowing selective response to HOCl generated in the MPO + H_2O_2 + NaCl system. Upon incubation with increasing concentrations of HOCl (or MPO-generated HOCl), polyacrylamide gel electrophoresis (PAGE, 10%) revealed progressive cleavage of pH2 (Figure S2). Two distinct bands corresponding to the intact strand and the cleaved product were

observed, with a gradual decrease in the intact band and a concomitant increase in the faster-migrating cleavage band as the oxidant level increased. This migration pattern is consistent with site-specific cleavage at the phosphorothioate-modified region, confirming the oxidative responsiveness and structural stability of pH2 prior to activation. These findings indicate that HOCl efficiently cleaves the PS site, removes the structural blockade, and converts pH2 into its active H2 form by exposing its toehold, thus unlocking the second gate. In Fig. 1e and f, we tested the amplification performance and input specificity of the CHA module. A basic reaction system containing H1, H2, and a fluorogenic reporter (FQ probe) was assembled. CHA was initiated by adding varying concentrations of the released T strand, alongside a mismatched T strand group and a blank control. As expected, fluorescence increased with T strand concentration, while the mismatched and control groups showed negligible signal, confirming that the CHA circuit is selectively activated and enables efficient signal amplification only in the presence of the correct trigger. The fluorescence spectra (Fig. 1g) further support the dose-dependent nature of the CHA response. PAGE was performed to validate the assembly and activation of the catalytic hairpin assembly (CHA) reaction under various combinations of trigger (T), hairpin H1, and hairpin H2 (Figure S3). Individual components or partial combinations produced only faint or low-molecular-weight bands, indicating minimal spontaneous hybridization in the absence of the complete reaction system. In contrast, the simultaneous presence of T, H1, and H2 resulted in the appearance of pronounced higher-molecular-weight bands, with increased band intensity observed at higher trigger concentrations, confirming effective CHA initiation and cascade assembly. Taken together, the results from Fig. 1 provide strong experimental validation for the modular functionality of the dual-lock biosensing system. The aptamer-mediated release of T, HOCl-induced activation of pH2, and the downstream CHA-based amplification cascade function synergistically and reliably within the proposed logic-gated architecture.

Construction and response evaluation of the dual-lock logic-gated DNA sensing system

To enable precise molecular recognition and signal transduction, we constructed a DNA nanodevice that integrates aptamer binding and oxidative cleavage within a dual-lock logic-gated architecture, capable of detecting active MPO. As shown in Fig. 2a, the sensing system incorporates two input-dependent control elements, corresponding to two molecular "keys." Input 1 (MPO): The trigger strand (T) is initially hybridized with the MPO-specific aptamer (Apt), forming a locked duplex that inhibits signal propagation. Only when MPO is present does it competitively bind the aptamer and release the T strand, enabling downstream activation of the CHA cascade. Input 2 (HOCl): HOCl, generated by MPO in the presence of H_2O_2 and Cl^-, selectively cleaves the internal PS site of the protected hairpin pH2. This cleavage disrupts the blocking segment and exposes the toehold of H2, converting pH2 into its active conformation. These two inputs act cooperatively to regulate signal output. Only when both the T strand and activated H2 are present can the CHA reaction proceed, fulfilling an AND logic gate function. To experimentally validate the logic behavior, Fig. 2b shows fluorescence spectra under different component combinations. Introducing only the T strand (FQ + H1 + pH2 + T) or T with MPO (FQ + H1 + pH2 + T + MPO) failed to induce significant fluorescence. In contrast, only when the full MPO catalytic system (MPO + H_2O_2 + Cl^-) was introduced did the system generate a strong fluorescence signal, confirming that both molecular locks must be disengaged for activation. Figure 2c provides the corresponding quantitative analysis of relative fluorescence intensity (R/R_0), clearly demonstrating the cooperative nature of the dual-input activation and the high specificity of the system.

Optimization of reaction conditions for the dual-lock MPO sensing system

To ensure the stability and sensitivity of the sensing system under practical conditions, we systematically evaluated the influence of several key environmental parameters, including pH, temperature, Cl^- concentration, and H_2O_2 concentration (Fig. 3). As shown in Fig. 3a, the fluorescence intensity peaked at pH 6.0, which aligns with the optimal catalytic activity of MPO under mildly acidic conditions. Alkaline pH (e.g., 9.2) significantly reduced the signal, indicating impaired enzymatic efficiency. Temperature also had a notable impact on the sensing response (Fig. 3b). The strongest fluorescence signal was observed at 37 °C, while lower signals were recorded at 25 °C and 30 °C. The signal at 42 °C was comparable to that at 37 °C, indicating that the system maintains optimal reactivity and structural stability near physiological temperature. Since MPO catalysis relies on both Cl^- and H_2O_2 as substrates, we next examined their concentration-dependent effects. As shown in Fig. 3c, the fluorescence signal increased with Cl^- concentration and plateaued at 20 mM, suggesting this concentration is sufficient to saturate MPO's catalytic requirement. Higher concentrations (≥ 40 mM) did not yield further enhancement, implying a reaction plateau. Similarly, Fig. 3d shows that the system exhibited the strongest fluorescence at 20 μM H_2O_2, with a stable signal range from 20 to 100 μM. In contrast, lower concentrations (5–10 μM) resulted in significantly weaker fluorescence, indicating that 20 μM is the threshold for effective MPO activation

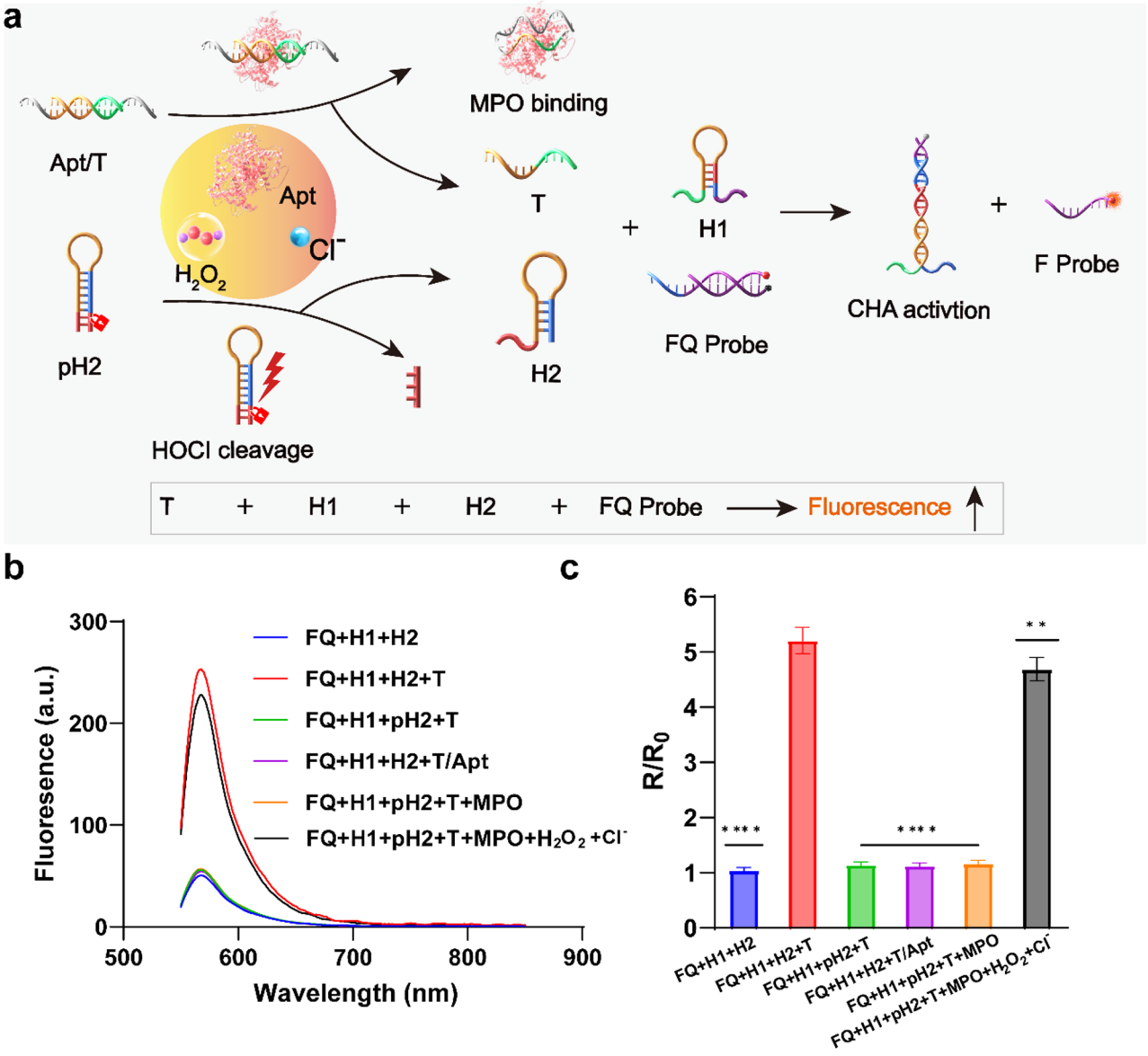

Fig. 2 Design and fluorescence verification of the dual-lock DNA logic gate. (**a**) Schematic representation of the dual-input sensing mechanism. Input 1: MPO binds the aptamer, releasing trigger T strand. Input 2: HOCl, generated by the MPO–H_2O_2–Cl^- system, cleaves pH2 to expose the H2 toehold. Only when both inputs are present is the CHA reaction activated, generating fluorescence. (**b**) Fluorescence spectra for different component combinations. Signal appears only under dual-input conditions, consistent with AND logic behavior. (**c**) Normalized fluorescence intensity (R/R_0) corresponding to panel (**b**). Significant signal enhancement is observed only with both MPO and catalytic substrates. *$p < 0.05$, **$p < 0.01$, ***$p < 0.001$, ****$p < 0.0001$

in this system. Taken together, the optimal conditions for the dual-lock sensing platform are: pH 6.0, temperature 37 °C, Cl^- 20–100 mM, and H_2O_2 20–100 μM. These parameters ensure robust performance of the sensor under physiologically relevant environments.

Analytical performance evaluation of the dual-lock fluorescent MPO sensing platform

To systematically evaluate the performance of the dual-lock logic-gated MPO sensing system, we assessed its specificity, sensitivity, quantification ability, and enzyme activity dependence, as summarized in Fig. 4. Specificity analysis was conducted using a range of protein and redox interferents. As shown in Fig. 4a and b, only catalytically active MPO in the presence of H_2O_2 and Cl^-, or exogenous MPO and HOCl, triggered a strong fluorescence response. Other conditions—including MPO alone, inactive MPO, or single substrates—produced negligible signals, confirming strict dual-input gating and minimal false positives. In Fig. 4c, further selectivity was demonstrated by testing structurally and functionally related biomolecules commonly encountered in oxidative stress environments, such bovine serum albumin (BSA), horseradish peroxidase (HRP), lactoperoxidase

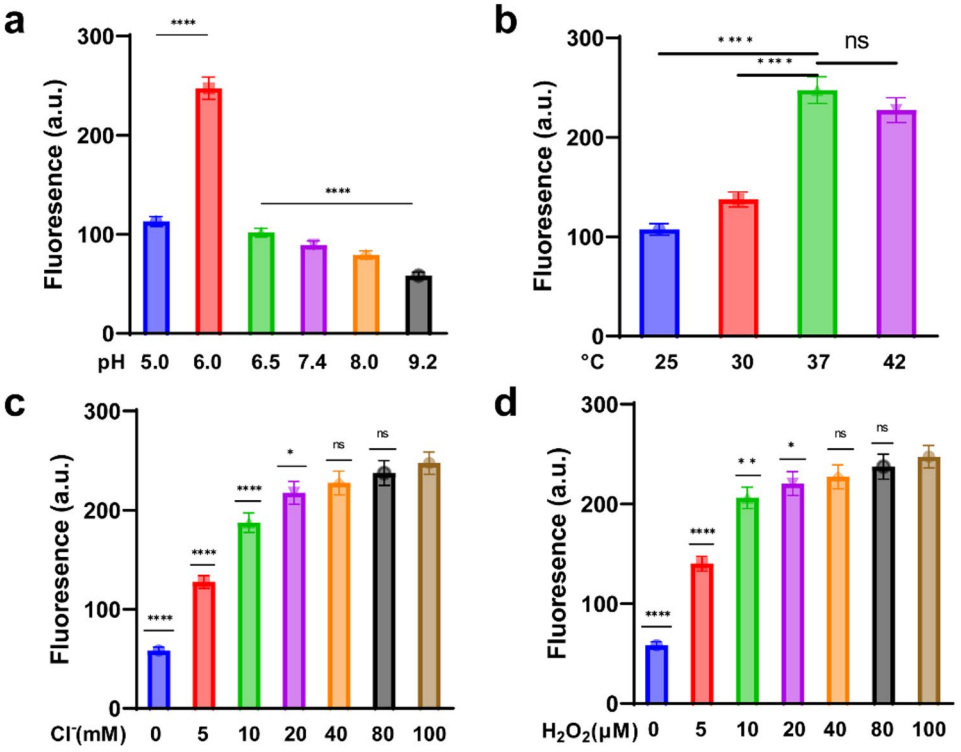

Fig. 3 Optimization of key reaction conditions for the dual-lock logic-gated MPO sensing system. (**a**) Fluorescence measurements under different pH conditions to evaluate the influence of acidity on system performance. (**b**) Assessment of fluorescence output at various incubation temperatures (25 °C, 30 °C, 37 °C, and 42 °C). (**c**) Fluorescence response as a function of Cl^- concentration ranging from 0 to 30 mM. (**d**) Evaluation of fluorescence intensity across a gradient of H_2O_2 concentrations (5–100 μM)

(LPO), NADPH, catalase (CAT), glucose oxidase (GOx), xanthine oxidase and glutathione reductase (GR). Only catalytically active MPO induced a significant fluorescence signal. This result confirms the high specificity of the system in discriminating MPO from structurally and functionally related oxidoreductases. Notably, the high specificity toward MPO arises from the synergistic dual-lock design combining aptamer recognition and HOCl-triggered chemical activation. Only MPO can effectively bind the aptamer to release the trigger strand and simultaneously generate sufficient HOCl to cleave the phosphorothioate-modified pH2. In contrast, other peroxidases such as HRP and LPO neither exhibit strong aptamer affinity nor produce HOCl at comparable levels under physiological conditions. As a result, unintended CHA activation is effectively suppressed, ensuring robust discrimination of MPO from related oxidoreductases. To further assess the anti-interference capacity of the platform, we conducted interference assays under physiologically relevant conditions (Fig. 4d). The system was challenged with a panel of redox-active species (e.g., cysteine, GSH, ascorbic acid), oxidants (e.g., HOCl, H_2O_2, NO_3^-), and abundant cations found in biological fluids (e.g., Na^+, K^+, Ca^{2+}, Mg^{2+}, Fe^{3+}). None of these interferents triggered notable fluorescence increases, while MPO consistently activated the system. These findings underscore the excellent selectivity and robustness of the platform under complex biological conditions.

We next assessed the sensitivity and dynamic range of the platform. As shown in Fig. 4e, the fluorescence intensity increased proportionally with MPO concentration from 0.5 to 30 ng/mL, forming a clear kinetic response profile. Endpoint fluorescence spectra (Fig. 4f) further validated this trend, showing dose-dependent enhancement centered at ~ 570 nm. A calibration curve was constructed based on endpoint intensity (Fig. 4g), exhibiting excellent linearity (R^2 = 0.9834) with the regression equation $Y = 9.023X + 43.34$. The limit of detection (LOD) was estimated to be 1.73 ng/mL. These results demonstrate the system's high sensitivity and broad dynamic range for quantitative MPO detection. To clarify the specificity of MPO-dependent activation, we evaluated the influence of alternative halide substrates and inhibitors on signal generation. As shown in Figure S4, chloride efficiently supported fluorescence activation, whereas bromide induced a non-monotonic response. In contrast, iodide and thiocyanate failed to produce appreciable fluorescence enhancement, indicating that their MPO-derived oxidants are insufficient to trigger efficient phosphorothioate cleavage. Moreover, inhibition of MPO by 4-aminobenzoic acid hydrazide (4-ABAH) resulted in a dose-dependent suppression of fluorescence

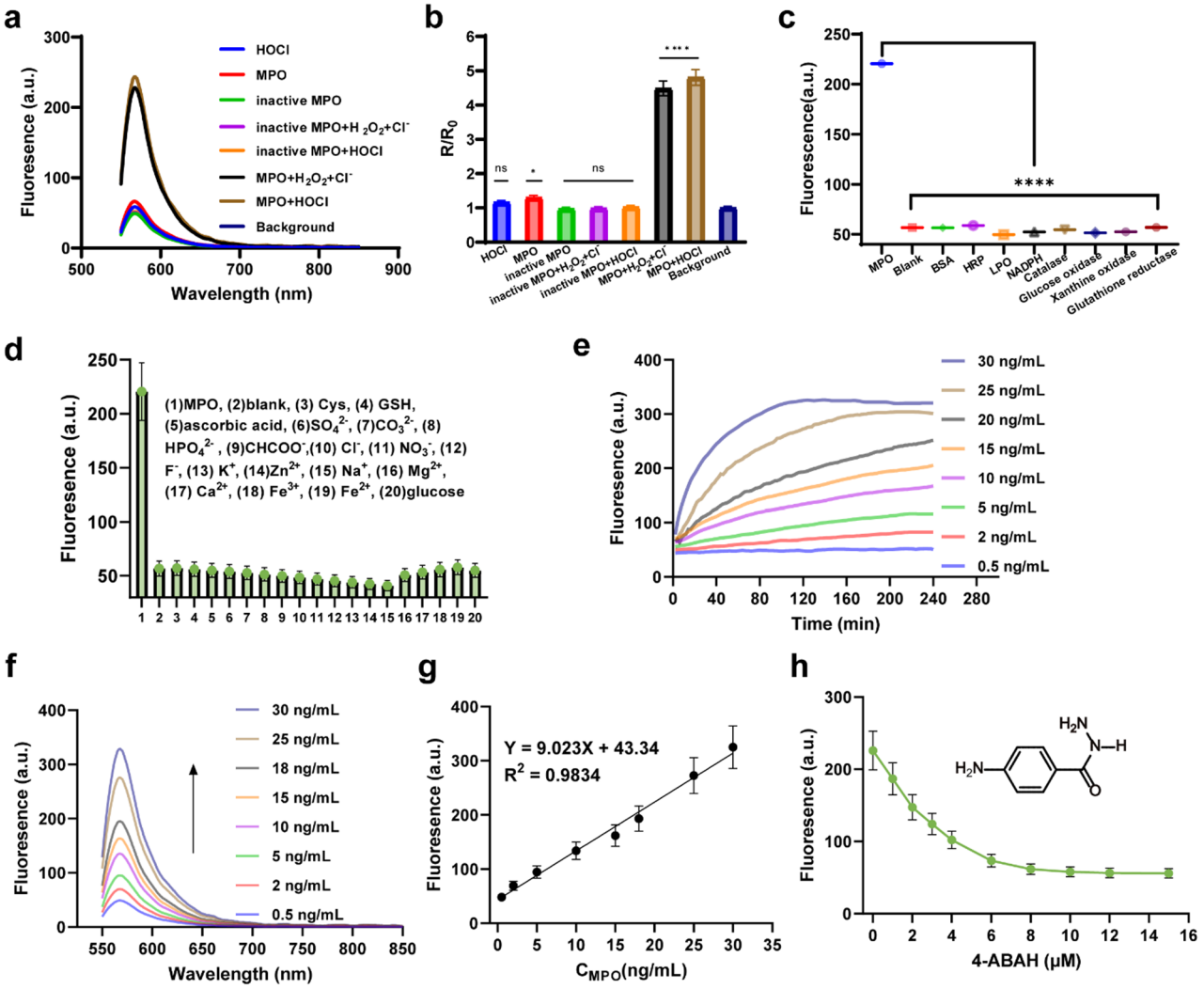

Fig. 4 Analytical performance evaluation of the dual-lock MPO fluorescent sensing platform. (**a**) Fluorescence spectra under seven representative biochemical conditions (e.g., MPO, inactive MPO, HOCl, partial combinations). (**b**) Quantified R/R_0 values from (**a**), highlighting selective activation by catalytically active MPO. Background corresponds to the condition containing only FQ-labeled H1 and pH2. (**c**) Fluorescence response of the system to various redox-related proteins and small molecules, including BSA, HRP, LPO, NADPH, CAT, GOx, xanthine oxidase, and GR. (**d**) Interference assessment under physiologically relevant conditions. Nineteen potential interfering substances—including reducing agents (Cys, GSH, ascorbic acid), oxidants (HOCl, H_2O_2, NO_3^-), and common metal cations (Na^+, K^+, Ca^{2+}, Mg^{2+}, Fe^{3+}). (**e**) Fluorescence kinetic curves at different MPO concentrations (0.5–30 ng/mL), showing dose-dependent signal amplification. (**f**) Steady-state fluorescence spectra corresponding to (**e**), with increasing emission intensities at ~570 nm in response to higher MPO concentrations. (**g**) Calibration curve based on endpoint fluorescence intensities. Linear relationship observed within 0.5–30 ng/mL ($R^2 = 0.9834$; $Y = 9.023X + 43.34$). (**h**) Fluorescence inhibition by MPO-specific inhibitor 4-ABAH. Signal intensity decreased with increasing 4-ABAH concentration (0–16 μM)

output (Fig. 4h), confirming that signal generation strictly depends on MPO catalysis. Taken together, the dual-lock fluorescent sensing platform exhibits outstanding performance in terms of specificity, sensitivity, quantitative accuracy, and interference resistance. These features highlight its potential for reliable detection of MPO content and activity in complex biological samples.

Recovery analysis in biological samples and long-term stability evaluation of the biosensor

The MPO aptamer employed in this work was previously selected and quantitatively characterized, exhibiting low-nanomolar to sub-nanomolar binding affinity and high specificity toward MPO under physiologically relevant buffer conditions. To further evaluate the applicability of the developed sensing platform in realistic biological environments, recovery experiments were performed in complex matrices including human serum, cell lysate, and saliva. Known concentrations of MPO (5, 10, and

15 ng mL^{-1}) were spiked into each matrix, and the corresponding fluorescence responses were recorded and summarized in Table S2. In all tested samples, the biosensor accurately quantified MPO with recoveries ranging from 99.78% to 106.42% and relative standard deviations (RSDs) below 4.85%, demonstrating excellent accuracy and reproducibility. Although detailed kinetic and ionic-strength dependence analyses were beyond the scope of this study, the consistently robust performance observed in these complex matrices indicates that the aptamer–MPO interaction and the downstream logic-gated sensing process are sufficiently tolerant to realistic ionic and matrix variations, underscoring the practical feasibility of the proposed sensing platform. To further investigate the long-term performance of the fluorescent biosensor, stability studies were carried out under refrigerated storage conditions (4 °C, protected from light) for up to six months. The sensor was stored under two conditions: in the presence and absence of MPO, and fluorescence responses were periodically measured. As illustrated in Figure S5, the fluorescence intensity in the MPO group remained consistently high over the 6-month period, with only a slight, non-significant decrease, indicating stable sensor performance over time. In contrast, the fluorescence signals in the control group without MPO remained at a low background level throughout the entire duration, showing no evidence of spontaneous signal activation. These results confirm the excellent storage stability and anti-background triggering capacity of the system. In summary, the proposed MPO biosensor exhibits high detection accuracy across various biological matrices and retains excellent stability under standard storage conditions. These properties make it highly suitable for preclinical sample analysis and long-term storage following batch fabrication.

Conclusion

In summary, we have established a dual-lock, logic-gated DNA biosensing platform that enables highly specific and concurrent detection of both the presence and enzymatic activity of myeloperoxidase (MPO), a key oxidative enzyme involved in inflammation-associated pathologies. By integrating aptamer-mediated target recognition with HOCl-triggered oxidative cleavage, the system operates under a stringent AND logic mechanism, generating signals only when both MPO binding and catalytic activity are present. This architecture effectively minimizes background leakage and false-positive responses from inactive MPO or related peroxidases. Under optimized conditions, the sensor exhibits a broad linear range (0.5–30 ng/mL), a low detection limit (~ 1.73 ng/mL), and robust performance in complex biological matrices, including human serum, saliva, and cell lysate. Owing to its modular, isothermal, and activity-dependent design, the platform is readily adaptable to practical diagnostic formats such as microfluidic chips, point-of-care devices, and automated high-throughput systems, thereby offering enhanced clinical reliability and translational potential. While the oxidative cleavage step may be sensitive to redox fluctuations in complex environments and warrants further optimization for in vivo applications, the DNA nanostructures employed—particularly the phosphorothioate-modified hairpins and aptamer–trigger complexes—demonstrate high reproducibility and minimal batch-to-batch variability due to standardized synthesis and handling procedures. Overall, this dual-lock strategy exemplifies the integration of programmable nucleic acid circuitry with biochemical reactivity, providing a versatile paradigm for next-generation biosensing and molecular logic–based diagnostics.

Supplementary Information

The online version contains supplementary material available at https://doi.org/10.1186/s12967-026-07780-4.

Supplementary Material 1

Acknowledgements
Not applicable.

Author contributions
All authors have had access to the data and all drafts of the manuscript. Specific contributions are as follows: Bo-Yu Shi: Writing – original draft, Investigation, Formal analysis, Data curation. Jia-Mei Zhang: Writing – review & editing, Validation, Methodology, Investigation, Formal analysis, Data curation. Si-Han Qin: manuscript drafting. Han-Ye Yuan: manuscript review. Jing Wang: Writing – review & editing, Writing – original draft, Validation, Supervision, Methodology, Funding acquisition, Formal analysis, Data curation, Conceptualization.

Funding
This research was supported by the Tianjin Education Commission research project (2023KJ074).

Data availability
The datasets used and analysed during the current study are available from the corresponding author on reasonable request.

Declarations

Ethics approval and consent to participate
Our research was approved by the local ethics committee based on the Declaration of Helsinki. The study was approved by the ethics committee of Tianjin Medical University, and written informed consent was obtained from each participant.

Consent for publication
All authors have reviewed and approved the final version of the manuscript for publication.

Competing interests
No conflict of interest was declared by the authors.

Received: 18 September 2025 / Accepted: 5 January 2026
Published online: 02 February 2026

References

1. Soleimany AP, Martin-Alonso C, Anahtar M, Wang CS, Bhatia SN. Protease activity analysis: A toolkit for analyzing enzyme activity data. ACS Omega. 2022;7:24292–301. https://doi.org/10.1021/acsomega.2c01559.
2. Ong ILH, Yang K-L. Recent developments in protease activity assays and sensors. Analyst. 2017;142:1867–81. https://doi.org/10.1039/C6AN02647H.
3. Chen K, Arnold FH. Engineering new catalytic activities in enzymes. Nat Catal. 2020;3:203–13. https://doi.org/10.1038/s41929-019-0385-5.
4. Montoya Mira JL, et al. Early detection of pancreatic cancer by a high-throughput protease-activated nanosensor assay. Sci Transl Med. 2025;17:eadq3110. https://doi.org/10.1126/scitranslmed.adq3110.
5. Rai P, et al. Protease detection in the biosensor era: A review. Biosens Bioelectron. 2024;244:115788. https://doi.org/10.1016/j.bios.2023.115788.
6. Davies MJ, Myeloperoxidase. Mechanisms, reactions and Inhibition as a therapeutic strategy in inflammatory diseases. Pharmacol Ther. 2021;218:107685. https://doi.org/10.1016/j.pharmthera.2020.107685.
7. Williams C, et al. Targeted Inhibition of myeloperoxidase (MPO): A new therapeutic strategy for the treatment of multiple myeloma. Blood. 2023;142:3319–3319. https://doi.org/10.1182/blood-2023-179196.
8. Gan P-Y, et al. Anti-CD20 mAb-Induced B cell apoptosis generates T cell regulation of experimental myeloperoxidase ANCA-Associated vasculitis. J Am Soc Nephrol. 2021;32:1071–83. https://doi.org/10.1681/asn.2020060834.
9. Wei H, et al. Multimodal tetrahedral DNA nanoplatform for surprisingly rapid and significant treatment of acute liver failure. Adv Mater. 2024;36:2305826. https://doi.org/10.1002/adma.202305826.
10. Chami B, Ahmad G, Schroder A, San Gabriel P, Witting P. the role of myeloperoxidase and neutrophil extracellular traps in the pathogenesis of inflammatory bowel disease. Gastroenterology. 2021;160:S5–6. https://doi.org/10.1053/j.gastro.2021.01.044.
11. Raskovalova T, et al. Flow cytometric analysis of peripheral blood neutrophil myeloperoxidase expression for ruling out myelodysplastic syndromes: a prospective validation study. Ann Hematol. 2021;100:1149–58. https://doi.org/10.1007/s00277-021-04446-7.
12. Khan AA, Alsahli MA, Rahmani AH. Myeloperoxidase as an active disease biomarker: recent biochemical and pathological perspectives. Med Sci. 2018;6:33.
13. Tan YJ, et al. iTRAQ-based proteomic analysis reveals myeloperoxidase (MPO) as a diagnostic and prognostic biomarker of cognitive decline in parkinson's disease. Alzheimer's Dement. 2023;19:e076988. https://doi.org/10.1002/alz.076988.
14. Valadez-Cosmes P, et al. Abstract 2823: exploring the role of neutrophil myeloperoxidase in lung cancer. Cancer Res. 2021;81:2823–2823. https://doi.org/10.1158/1538-7445.Am2021-2823.
15. Mihalic ZN, et al. Myeloperoxidase enhances the migration and invasion of human choriocarcinoma JEG-3 cells. Redox Biol. 2023;67:102885. https://doi.org/10.1016/j.redox.2023.102885.
16. Valadez-Cosmes P, Raftopoulou S, Mihalic ZN, Marsche G, Kargl J. Myeloperoxidase: growing importance in cancer pathogenesis and potential drug target. Pharmacol Ther. 2022;236:108052. https://doi.org/10.1016/j.pharmthera.2021.108052.
17. Shamsuzzaman S, et al. Novel mouse model of myocardial Infarction, plaque Rupture, and stroke shows improved survival with myeloperoxidase Inhibition. Circulation. 2024;150:687–705. https://doi.org/10.1161/circulationaha.123.067931.
18. Ramachandra CJA, et al. Inhibiting cardiac myeloperoxidase alleviates the relaxation defect in hypertrophic cardiomyocytes. Cardiovasc Res. 2022;118:517–30. https://doi.org/10.1093/cvr/cvab077.
19. Nandeshwar R, Tallur S. Electrochemical detection of myeloperoxidase (MPO) in blood plasma with surface-modified electroless nickel immersion gold (ENIG) printed circuit board (PCB) electrodes. Biosens Bioelectron. 2024;246:115891. https://doi.org/10.1016/j.bios.2023.115891.
20. Tian F, et al. A HClO-specific near-infrared fluorescent probe for determination of myeloperoxidase activity and imaging mitochondrial HClO in living cells. Biosens Bioelectron. 2016;86:68–74. https://doi.org/10.1016/j.bios.2016.06.039.
21. Permpoka K, et al. Smartphone-enabled 3D origami-fluidic paper-based electrochemical detection of myeloperoxidase activity for assessing wound infection. Sens Actuators B. 2024;398:134712. https://doi.org/10.1016/j.snb.2023.134712.
22. Wang C, et al. A versatile imaging platform with fluorescence and CT imaging capabilities that detects myeloperoxidase activity and inflammation at different scales. Theranostics. 2019;9:7525–36. https://doi.org/10.7150/thno.36264.
23. Chen Y, et al. Myeloperoxidase-mimetic nanozyme generates hypochlorous acid for phagosomal bacteria elimination. Nano Today. 2024;54:102137. https://doi.org/10.1016/j.nantod.2023.102137.
24. Gau J, et al. Flavonoids as promoters of the (pseudo-)halogenating activity of lactoperoxidase and myeloperoxidase. Free Radic Biol Med. 2016;97:307–19. https://doi.org/10.1016/j.freeradbiomed.2016.06.026.
25. Panasenko OM, Torkhovskaya TI, Gorudko IV, Sokolov AV. The role of halogenative stress in atherogenic modification of Low-Density lipoproteins. Biochem (Moscow). 2020;85:34–55. https://doi.org/10.1134/S0006297920140035.
26. Guo J-Y, et al. One-step screening of myeloperoxidase aptamer using porous PEG hydrogel. Adv Compos Hybrid Mater. 2025;8:244. https://doi.org/10.1007/s42114-025-01319-9.
27. Wang J, et al. Oxidative cleavage-based three-dimensional DNA biosensor for ratiometric detection of hypochlorous acid and myeloperoxidase. Anal Chem. 2021;93:16231–9. https://doi.org/10.1021/acs.analchem.1c04113.
28. Ma J-Y, et al. CRISPR/Cas12a-based hypochlorous acid and myeloperoxidase biosensors designed on RESET effect. Sens Actuators B. 2023;376:133000. https://doi.org/10.1016/j.snb.2022.133000.
29. Hu Z, et al. Site-Specific scissors based on myeloperoxidase for phosphorothioate DNA. J Am Chem Soc. 2021;143:12361–8. https://doi.org/10.1021/jacs.1c06370.
30. Ji M, et al. Endogenous HClO-Gated cascade MicroRNA imaging for precise diagnosis of atherosclerosis in vivo. J Am Chem Soc. 2025;147:7113–26. https://doi.org/10.1021/jacs.5c00031.
31. Kabza AM, Young BE, Sczepanski JT, Heterochiral. DNA strand-displacement circuits. J Am Chem Soc. 2017;139:17715–8. https://doi.org/10.1021/jacs.7b10038.
32. Zhu L, Yu L, Yang X. Electrochemiluminescence cascade amplification platform for detection of Dual-microRNA and operation of concatenated logic circuit. Anal Chem. 2022;94:17279–86. https://doi.org/10.1021/acs.analchem.2c04242.
33. Zhu L, et al. Label-free electrochemical sensing platform for sensitive detection of ampicillin by combining nucleic acid isothermal enzyme-free amplification circuits with CRISPR/Cas12a. Talanta. 2024;273:125950. https://doi.org/10.1016/j.talanta.2024.125950.

Publisher's note